ORIGINAL ARTICLE

Decadal variability of MJO teleconnections in a coupled climate model

Daniel T. Skinner[1,2] | **Adrian J. Matthews**[2,3] | **David P. Stevens**[3]

[1]Climatic Research Unit, School of Environmental Sciences, University of East Anglia, Norwich, United Kingdom

[2]Centre for Ocean and Atmospheric Sciences, School of Environmental Sciences, University of East Anglia, Norwich, United Kingdom

[3]Centre for Ocean and Atmospheric Sciences, School of Engineering, Mathematics and Physics, University of East Anglia, Norwich, United Kingdom

Correspondence
D. T. Skinner, Climatic Research Unit, School of Environmental Sciences, University of East Anglia, Norwich Research Park, NR4 7TJ, Norwich, United Kingdom
Email: D.Skinner@uea.ac.uk

Funding information
Natural Environment Research Council, Grant/Award Number: NE/R016704/1 (TerraMaris). University of East Anglia, Faculty of Science Studentship.

KEYWORDS
Madden–Julian Oscillation, Teleconnection, Atlantic Multi-decadal Variability, Pacific Decadal Oscillation, Climate Model, North Atlantic Oscillation, Stratospheric Polar Vortex

Abstract

The Madden—Julian Oscillation (MJO) is a key source of predictability for global weather. Through both tropospheric and stratospheric teleconnection pathways, the MJO is able to alter the the extratropical circulation, and in turn cause shifts in other modes of variability such as the Pacific—North American Pattern and North Atlantic Oscillation. MJO teleconnections are known to vary on a range of time scales, but their variability on decadal and multi-decadal time scales is not well understood. Using the UKESM1 coupled climate model, we show that both Atlantic Multi-decadal Variability (AMV) and the Pacific Decadal Oscillation (PDO) alter MJO teleconnection patterns and their impact on extratropical modes of variability.

AMV and the PDO modulate the mean state of the atmosphere, in particular the Aleutian Low, which controls how the circulation responds to the MJO. When the Aleutian Low is deepened, for example during the positive phase of the PDO, this provides the conditions necessary for the MJO teleconnection to project onto the climatological low, either constructively or destructively. During the positive phase of the AMV and negative phase of the PDO, which favour a weak Aleutian Low, the MJO cannot drive a significant cyclonic response in the region. Changes in the Stratospheric Polar Vortex, preceded by MJO related anomalies in the Aleutian Low, also control extratropical weather. We hypothesise that this stratospheric teleconnection pathway is also modulated by both AMV and the PDO. These results have implications for improving the predictability of extratropical weather patterns over the coming decades. By understanding how MJO teleconnections are altered by internal modes of decadal and multi-decadal variability, the impact of anthropogenic climate change can be better identified in future projections. This context will improve both long-range forecasts of MJO-driven variability, and short-term forecasts in different SST conditions.

1 | INTRODUCTION

Subseasonal atmospheric variability in the tropics is dominated by the Madden–Julian Oscillation (MJO; Madden and Julian, 1971, 1972; Jiang et al., 2020), a large-scale weather system where enhanced and suppressed convective anomalies propagate eastward through the tropics. The MJO is a key driver of weather in the extratropics, acting through two distinct teleconnection pathways (Barnes et al., 2019). A tropospheric teleconnection pathway forms when upper tropospheric divergence is triggered by anomalous MJO convection, in turn inducing a Rossby wave train which extends across the mid-latitudes into the extratropics (Matthews et al., 2004). This Rossby wave train can then project onto extratropical modes of variability such as the Pacific–North American Pattern (PNA; Franzke et al., 2011) and North Atlantic Oscillation (NAO; Hurrell et al., 2003). A stratospheric teleconnection pathway to the North Atlantic is also provided by a deepening of the Aleutian Low whilst enhanced MJO convection is centred over the West Pacific, which weakens the Stratospheric Polar Vortex (SPV; Waugh and Polvani, 2010) through increased vertical wave activity (e.g. Jiang et al., 2017). The deceleration of the SPV, in turn, favours the negative phase of the NAO (Woollings et al., 2010). The tropospheric teleconnection pathway is the dominant mechanism by which the MJO influences the extratropical circulation at lags of up to two weeks, however the stratospheric pathway is still of interest, particularly at lead times of 1–3 weeks (e.g. Garfinkel et al., 2012, 2014; Green and Furtado, 2019).

The behaviour of the MJO and its teleconnections vary over a range of time scales. The MJO exhibits variability on interannual (e.g. Pohl and Matthews, 2007) and decadal (e.g. Fu et al., 2020) time scales. Meanwhile, MJO teleconnections are modulated on sub-seasonal time scales by the propagation speed of the MJO (Yadav and Straus, 2017), and on interannual time scales by the Quasi-Biennial Oscillation (QBO; e.g. Feng and Lin, 2019) and the El Niño–Southern Oscillation (ENSO; e.g. Lee et al., 2019; Arcodia and Kirtman, 2023). The decadal variability of MJO teleconnections has been demonstrated by Skinner et al. (2023); however, the drivers of this variability are not currently well understood.

Atlantic Multi-decadal Variability (AMV) is the dominant global mode of low-frequency climatic variability (e.g. Grossmann and Klotzbach, 2009; Lin and Qian, 2022). It is defined as variability in North Atlantic mean SSTs, relative to the global average, and has a period of approximately 60–80 years. During its positive phase (AMV+), sea surface temperature (SST) anomalies in the North Atlantic are warmer than the global average, whilst the negative phase (AMV–) is characterised by cold SST anomalies compared to the global average.

The Pacific Decadal Oscillation (PDO) is the leading mode of SST variability in the North Pacific (e.g. Mantua and Hare, 2002; Newman et al., 2016). It is defined as the first empirical orthogonal function (EOF) of monthly-mean

SST anomalies across the North Pacific basin, and has a period of approximately 20–30 years. The positive phase (PDO+) is characterised by cold SST anomalies in the western and central North Pacific, with warm anomalies in the eastern North Pacific. The negative phase (PDO−) displays the opposite SST anomalies. The SST pattern exhibited by the PDO is similar to that of ENSO. PDO+ and El Niño both show similar cold anomalies in the western North and South Pacific, with warm anomalies in the eastern and tropical Pacific. The PDO differs from ENSO in its time scale – decadal rather than interannual – and in its meridional extent. Where ENSO is largely confined to the tropics, the PDO displays a (meridionally) wider equatorial tongue, and has its largest SST anomalies in the North, rather than equatorial Pacific (Mantua and Hare, 2002).

The modes introduced above are known to interact with each other, however these interactions have been studied to varying degrees. AMV and the PDO are inherently linked as large-scale modes of decadal SST variability, however they are generally treated as distinct modes. Zhang and Delworth (2007) demonstrate that the PDO is, in part, forced by AMV with an approximate 12-year lag, however this coupling between the modes is overestimated by the UKESM1 climate model, as discussed in Sections 2 and 3. The interaction between decadal modes of variability and MJO teleconnections is poorly understood at present, with Skinner et al. (2023) providing the first analysis of decadal variability in MJO teleconnections and Dong et al. (2025) linking the PDO to precipitation variability in the Southwestern United States.

Skinner et al. (2023) and Dong et al. (2025) both hypothesise that low-frequency modes of SST variability, such as AMV and the PDO, modulate the extratropical response to the MJO. Their respective analyses are, however, limited by the small sample of AMV and PDO oscillations during the observational time period they both study. Here this hypothesis is tested using a 1,100-year pre-industrial control simulation of an Earth system model thereby providing a considerably large sample size than previous studies. Whilst biases and inaccuracies in the model must be noted, this long-time simulation allows us to robustly interrogate the impact of each decadal SST mode on MJO teleconnections in a way that is not possible using the much shorter observational reanalysis datasets.

2 | THE UKESM1 MODEL

The UK Earth System Model (UKESM1.0-LL; henceforth simply UKESM1) is a model developed by the UK Met Office and National Environmental Research Council. Its pre-industrial control (piControl) simulation forms part of the core (DECK) suite of simulations from the CMIP6 project (Eyring et al., 2016). In the piControl simulation, forcings (aerosols, volcanic activity, land use, etc.) are held constant at 1850 levels[1] (Eyring et al., 2016). The simulation is run for 1,100 years, not including a 6,500 year total spin-up (5,000 year ocean-only spin-up, followed by a 1,000 year land-only spin-up, followed by a 500 year coupled spin-up). For a full evaluation of the model, and in particular the piControl simulation, see Section 4.1 of Sellar et al. (2019).

General circulation models consistently under-represent both MJO variability (e.g. Le et al., 2021), and tropical–extratropical teleconnections (e.g. Skinner et al., 2022; Williams et al., 2023). A common weakness in climate models over recent decades has been the excessive termination of MJO events over the Maritime Continent, producing a barrier effect (e.g. Ling et al., 2019; Zhou et al., 2023) which hinders skilful prediction of teleconnection patterns (Bao and Hartmann, 2014). Ahn et al. (2020) show that UKESM1 has a reasonable representation of trans-Maritime Continent propagation compared to other CMIP6 models, and outperforms the HadGEM3 model (the physical model which forms the basis of UKESM1). Whilst there is some weakening of the convective anomaly as the MJO passes over the Maritime Continent – which is to be expected in a model (Ahn et al., 2020), and may lead to a weaker response

[1] Or some pre-defined reference level – see Appendix A1.2 of Eyring et al. (2016).

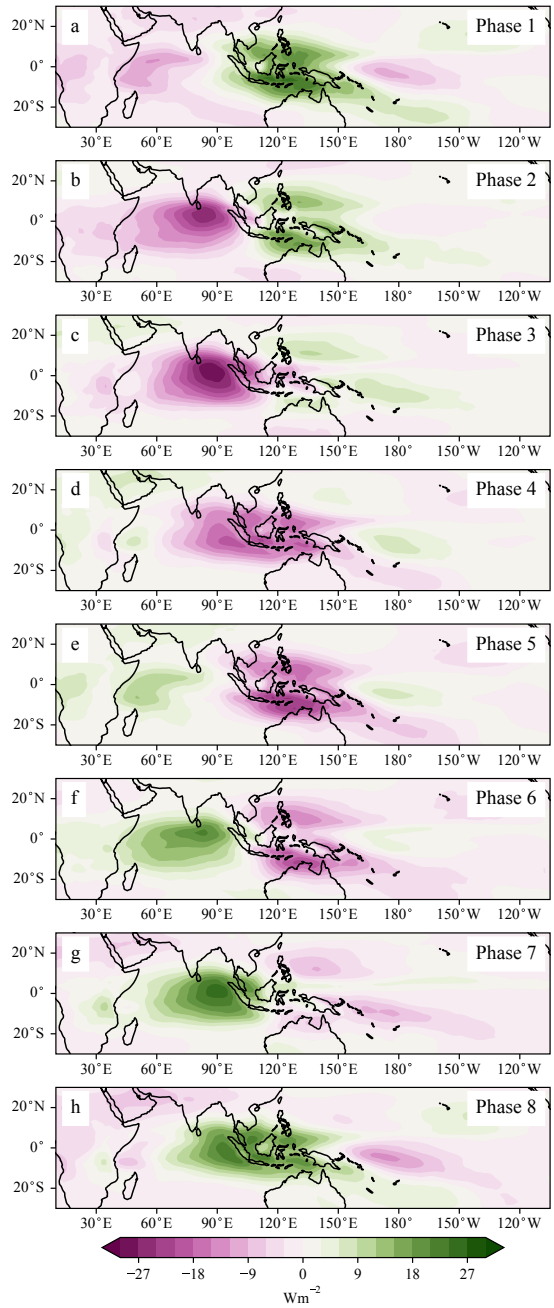

FIGURE 1 November–April outgoing long-wave radiation anomaly composites for each MJO phase in the UKESM1 pre-industrial control simulation. Pink shading (negative anomalies) indicates enhanced anomalous convection.

to later MJO phases (e.g. phase 6) – the MJO is able to successfully propagate without stalling (Figure 1e—g).

Stratospheric processes such as the SPV and sudden stratospheric warmings are represented with a range of fidelity across climate models (e.g. Wu and Reichler, 2020; Hall et al., 2021). UKESM1 has a well resolved stratosphere (85 vertical model levels, of which 35 are above 18km, and a fixed 85km model top (Walters et al., 2019)), compared to many other climate models (Sellar et al., 2019), and is able to outperform the HadGEM model in its representation of the SPV (Robson et al., 2020). The SPV is too weak in early winter (by up to ~40%) and too strong in late winter (by ~20%; see Robson et al., 2020, Figure 5), although this is a common feature of climate models (e.g. Seviour et al., 2016). Since MJO teleconnections display considerably seasonality (Esteva-Ingram, 2023), it is possible that this slight bias in SPV seasonality could carry through into a seasonality bias in the MJO teleconnection. This is a subject which could provide an interesting route for further study, but is beyond the scope of this work.

UKESM1 generally simulates low frequency SST variability well compared to other Earth system models (Coburn and Pryor, 2021). Robson et al. (2020) found that whilst North Atlantic SST variability is well represented in UKESM1 when compared with reanalysis data, model AMV (Figure 2a,c) explains a smaller proportion of global SST variability than observed AMV. This is likely because the model AMV is more closely correlated with global mean SST compared to reanalysis. The North Pacific SST anomalies associated with the PDO are more tightly concentrated around the Kuroshio–Oyashio extension (KOE) region in the model than in observations (Figure 2b,d). This difficulty with transporting SST anomalies across the Pacific is a long-standing issue for climate models (e.g. Pierce et al., 2001) and leads to excessive coupling between AMV and the PDO (Zhang and Delworth, 2007). Since SST biases in the KOE region are intimately linked with biases in jet position (Zhou and Xie, 2017), it is likely that the representation of MJO-induced Rossby waves will be affected by this bias. This highlights the limitations of using climate models in such analyses, and motivates comparison with observation/reanalysis-based studies such as Skinner et al. (2023) and Dong et al. (2025).

Overall the model does a relatively good job of representing decadal modes of variability individually (Sellar et al., 2019), but overestimates the link between the AMV and PDO (Coburn and Pryor, 2021). We are, however, able to address this issue (see section 3) by removing instances in which both modes are active simultaneously from our analysis, and in so doing consider the modes as independent. In summary, UKESM1 does suffer from some common limitations in its ability to simulate the MJO, SPV, and teleconnections, however this variability is reasonably well represented compared to other models (Sellar et al., 2019; Robson et al., 2020; Ahn et al., 2020).

3 | METHODOLOGY

The MJO is described using the real-time multi-variate MJO (RMM) index of Wheeler and Hendon (2004). Outgoing long-wave radiation (OLR), 850-hPa zonal wind ($U850$), and 250-hPa zonal wind ($U250$)[2] anomaly data from the model are generated by removing the mean and first three harmonics of the annual cycle. These anomalies are then 20–200 day band-pass filtered, before being projected onto the reanalysis-based EOF patterns calculated by Wheeler and Hendon. From the resulting RMM time series, each day in the 1100 year control run is assigned an MJO phase and amplitude. Phases 2–3 signify enhanced convection over the eastern Indian Ocean and suppressed convection over the western Pacific, phases 4–5 describe enhanced convection over the Maritime Continent and suppressed convection over the central Pacific and western Indian Ocean, phases 6–7 correspond to enhanced convection over the western Pacific and suppressed convection over the central to eastern Indian Ocean, and phases 8–1 denote enhanced convection over the central Pacific and western Indian Ocean and suppressed convection over the Maritime

[2] 250-hPa zonal wind data are used in place of 200-hPa zonal wind for RMM index calculation due to data availability constraints. This has negligible effect on the representation of the MJO or its teleconnections (Skinner et al., 2022).

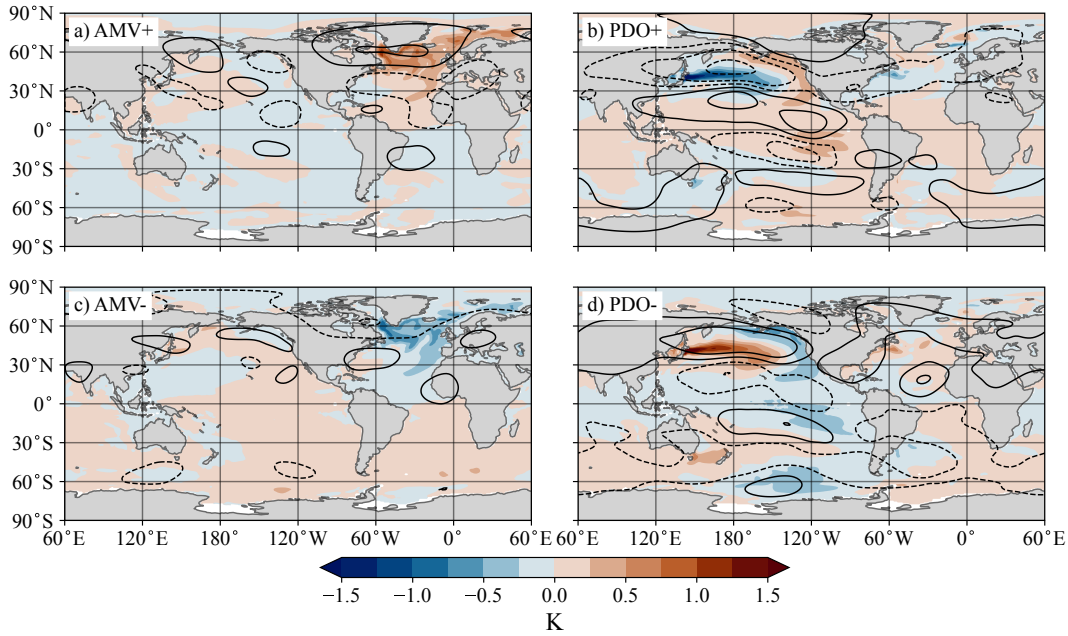

FIGURE 2 November–April composites of SST and $\psi 250$ anomalies for (a) AMV+, (b) PDO+, (c) AMV−, and (d) PDO−, in the UKESM pre-industrial control simulation. Colour shading shows the SST anomalies, whilst the black contours show the $\psi 250$ anomalies at $\pm 0.5 \times 10^6$ m^2 s^{-1}, $\pm 1.5 \times 10^6$ m^2 s^{-1}, and $\pm 3 \times 10^6$ m^2 s^{-1}. Dashed contours represent negative values.

Continent (Figure 1). The MJO is said to be active when the amplitude exceeds one, otherwise it is inactive or 'weak' and is not associated with any particular phase (Wheeler and Hendon, 2004).

The index of Trenberth and Shea (2006) is used to describe AMV. SST anomalies are averaged over the North Atlantic (80° W–0° E, 0–80° N), with the global average SST anomaly then subtracted. This time series is 10-year low-pass filtered, and is normalised to unit standard deviation. The PDO is defined as the first EOF of SST anomalies in the North Pacific (northward of 20° N), as described by Mantua et al. (1997). The EOF loading pattern is provided by the NOAA PSL, and is based on HadISST data. As with the AMV index, the time series is 10-year low-pass filtered, and is normalised to unit standard deviation.

AMV and the PDO are in their positive (negative) phase when their index value is greater than one (less than minus one) – that is when the magnitude of SST anomalies exceeds one standard deviation. When the respective index value has magnitude less than one, AMV and the PDO are said to be in their neutral phase (denoted AMV*n* and PDO*n*, respectively). Each November–April boreal winter season is then given an AMV and PDO designation, as described above, based on the mean value of the index across the season. As the model does not fully capture the relative variability of AMV and the PDO, we seek to separate the two modes. To achieve this, when compositing over one mode, the other is required to be neutral. For example, rather than compositing over all AMV+ seasons, we only consider those seasons which are both AMV+ and PDO*n*. Henceforth, references to, for example, AMV+ will assume PDO*n* implicitly. Whilst the size of the sample for each composite is reduced by this restriction, we are still left with a large enough sample for a robust analysis (Tables S1 and S2). Only boreal winter (November–April) seasons are considered throughout, since this is when both the MJO and its teleconnections are most active (Stan et al., 2017;

Jenney et al., 2019).

Lagged composites of 250-hPa streamfunction ($\psi 250$) anomaly are calculated for each MJO phase by averaging over all days in which the MJO is in the given phase and is active (lagged by a given number of days). For different SST states, composites are then calculated by further subsetting on winter seasons with the given AMV or PDO sign. The $\psi 250$ anomalies are calculated relative to the mean state of the whole time domain, however we would expect a different mean state for a subset of the time domain. Hence, to see the response to the MJO (conditional on a given SST state), rather than the combined response to the MJO and the decadal SST variability, we subtract the mean $\psi 250$ anomaly field for the given SST state from all composites. For example, the lagged composite of $\psi 250$ anomaly for MJO phase 6 in AMV+ is the lagged composite of $\psi 250$ anomaly over all days in which, simultaneously, the MJO is in phase 6 and AMV is in its positive phase (and the PDO is neutral), minus the composite of $\psi 250$ anomaly over all days in which AMV is in its positive phase (regardless of MJO phase).

To calculate the strength of the SPV, boreal winter zonal mean 50-hPa geopotential height ($Z50$) anomalies are averaged over 60–90° N (Waugh and Polvani, 2010). Polar cap $Z50$ anomalies are then composited by the aforementioned SST regimes and MJO phases at a range of lags, to assess the lagged dependence of the SPV on the MJO. To fully diagnose changes in the stratospheric teleconnection pathway would require analysis of changes in vertical wave activity as a result of Aleutian Low variability, the subsequent impact of this wave activity on the SPV, and then the downward propagation of these stratospheric circulation changes into the troposphere. This goes beyond the scope of this study, so we present MJO composites of SPV strength to make hypotheses, based on established physical mechanisms, about the changes to the stratospheric pathway.

Statistical significance is assessed throughout through the use of two-tailed t-tests at the 90% confidence level. Since each MJO phase is active for approximately 3–5 days, (Skinner et al., 2022), and the NAO has a decorrelation time scale of approximately 5–6 days (Domeisen et al., 2018), we reduce the number of degrees of freedom in our significance testing (Table S2) by a factor of 5 to account for autocorrelation [3].

4 | RESULTS

The extratropics respond to all phases of the MJO. However, phases 3 and 6 produce the clearest signal in both the North Pacific and North Atlantic (e.g. Cassou, 2008; Skinner et al., 2022). The responses to these particular MJO phases are well documented, so for the sake of clarity, we focus on these two phases. We also focus on the Northern Hemisphere in our discussion, since MJO teleconnections are strongest in the winter (in this case Northern) Hemisphere.

4.1 | Response to MJO phase 6

MJO phase 6 is characterised by enhanced MJO convection over the eastern Maritime Continent and western Pacific (Figure 1f). As a result of this enhanced convection, a Rossby wave-train is initiated, which propagates into the extratropics, deepening the Aleutian Low and causing a shift to negative NAO and positive PNA (e.g. Cassou, 2008; Seo and Lee, 2017). The deepening of the Aleutian Low additionally leads an increase in vertical wave activity, thereby disrupting and weakening the SPV (Waugh and Polvani, 2010). This weakening of the SPV can then propagate downwards into the troposphere to induce a negative NAO (Woollings et al., 2010).

Changes in either the tropical MJO forcing (e.g. Yadav and Straus, 2017), the extratropical mean state through

[3] The results are not qualitatively sensitive to the exact choice of decorrelation time scale.

which the Rossby wave propagates (e.g. Henderson et al., 2017), the SPV (e.g. Barnes et al., 2019), or some combination of these factors (e.g. Arcodia and Kirtman, 2023; Yadav et al., 2024) will alter the resultant teleconnection. Hence we examine each of these aspects to determine which are affected by decadal scale SST changes.

4.1.1 | Changes in tropical MJO forcing

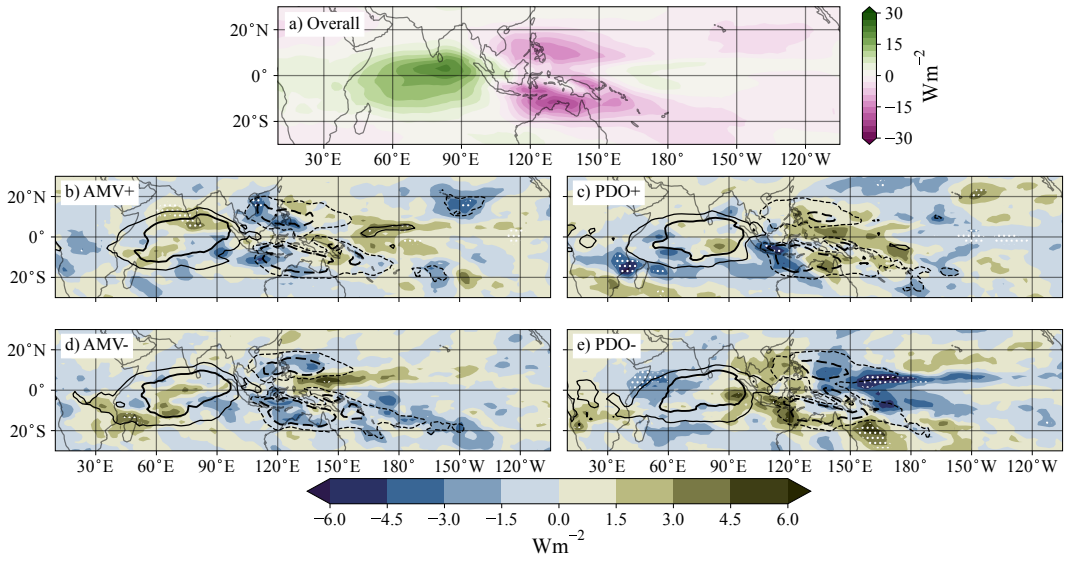

FIGURE 3 (a) MJO phase 6 composite (lag 0) of OLR anomalies, calculated over the whole northern winter data set, as in panel Figure 1f. (b–e) MJO phase 6 composite of OLR anomalies as a result of conditioning on the given SST regime: (b) AMV+, (c) PDO+, (d) AMV−, and (e) PDO−. The change in the OLR anomaly from the overall pattern in (a) is shown by the colour shading. The actual OLR anomalies are shown by the black line contours, plotted at $\pm 6\,W\,m^{-2}$ and $\pm 6\,W\,m^{-2}$. Dashed contours represent negative values. Stippling denotes regions in which the SST conditioned anomaly is significantly different from the overall anomaly at the 90% confidence level.

Whilst there are coherent changes in the tropical OLR anomalies associated with the MJO (Figure 3), these changes are not generally statistically significant, and are not consistent with the underlying SST anomalies (Figure 2). For example, during PDO− we see an eastward extension of the MJO convective anomaly (blue shading around 150–180° E in Figure 3e), whereas we would expect the opposite due to cooler SSTs in the eastern tropical Pacific (Figure 2d; Kessler, 2001). Also, the changes in MJO convection are not asymmetric for both decadal modes – that is, the changes as a result of AMV+ do not mirror the changes as a result of AMV−. Based on this range of evidence, we may conclude that most of the changes in MJO convective anomalies are simply noise as they do not meet the 90% threshold for statistical significance.

There is a significant strengthening of the anticyclonic response to tropical MJO heating (≈ 20° N, 160° E) initiated by the MJO during AMV− (coloured shading in Figure 4d). This coincides with a Rossby wave-like change in the circulation response stretching across the extratropics (beginning ≈ 20° N, 160° E, crossing North America and into the North Atlantic around 30–40° N) which, in a linear Rossby wave framework (e.g. Li et al., 2015; Deb et al., 2020), could be interpreted as a shift in the favoured Rossby wave modes being excited by MJO-related upper tropospheric

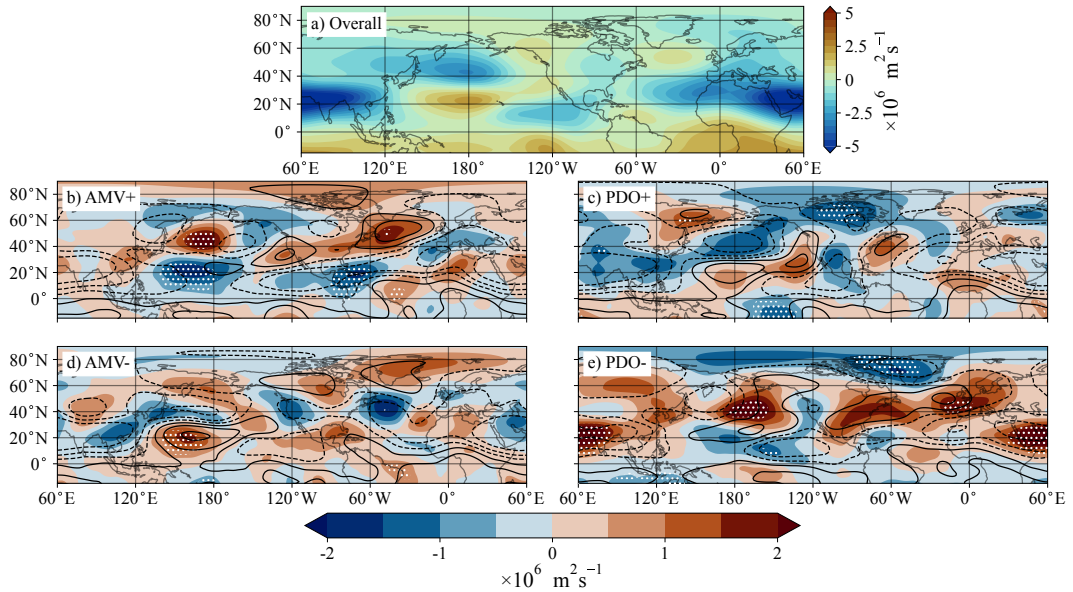

FIGURE 4 (a) 10-day lagged MJO phase 6 composite of $\psi 250$ anomalies, calculated over the whole northern winter data set. (b–e) 10-day lagged MJO phase 6 composite of $\psi 250$ anomalies as a result of conditioning on the given SST regime: (b) AMV+, (c) PDO+, (d) AMV−, and (e) PDO−. The change in the $\psi 250$ anomaly from the canonical pattern in (a) is shown by the colour shading. The actual $\psi 250$ anomalies are shown by the black line contours, plotted at $\pm 0.5 \times 10^6$ m^2 s^{-1}, $\pm 1.5 \times 10^6$ m^2 s^{-1}, and $\pm 3 \times 10^6$ m^2 s^{-1}. Dashed contours represent negative values. Stippling denotes regions in which the SST conditioned response is significantly different from the overall response at the 90% confidence level.

divergence (in this case to a higher wavenumber). This is comparable to the findings of Dong et al. (2025), who show that over the past two to three decades the MJO has tended to excite a wavenumber-5 Rossby wave response which was not present in the decades prior (though they attribute this change to the PDO rather than AMV, which also switches sign over the time periods studied.) Since this wave-like change does not project directly onto either the overall response or the response during AMV−, the modification does not result in a simple strengthening or weakening of the teleconnection, however this does highlight the highly non-linear nature of the SST modulation of the response.

4.1.2 | Changes in the extratropics as a result of mean state changes

The UKESM1 model can reproduce the deepened Aleutian Low that we would expect to see after MJO phase 6 (Figure 4a; ≈50° N, 180° E; Figure S1a). However, the expected positive PNA response (Seo and Lee, 2017) is less well simulated. Though a PNA-like quadrupole pattern is visible in the North Pacific region (cyclonic anomalies at 50° N, 180° E and 15° N, 120° W, and anticyclonic anomalies at 25° N, 180° E and 50° N, 120° W) these centres are shifted considerably to the West relative to the observed PNA (e.g. Franzke et al., 2011, ,Figure 1). In the North Atlantic, the UKESM1 model well represents the expected negative NAO response (Cassou, 2008), evident in the anticyclonic (55° N, 30° W) and cyclonic (30° N, 20° W) anomalies present in Figure 4a.

The expected deepening of the Aleutian Low due to MJO phase 6 is disrupted during AMV+ (Figures 4b, S1b).

A cyclonic upper-tropospheric circulation anomaly still occurs over the North Pacific (dashed line contours at 45° N, 160° W in Figure 4b) 10 days after MJO phase 6 when AMV is in its positive phase, however this circulation anomaly does not project well onto the canonical low anomaly for MJO phase 6 (blue shading at 40° N, 180° W in Figure 4a; Seo and Lee, 2017). This altered circulation response to MJO phase 6 is closer to the expected circulation response to AMV+, which displays a cyclonic anomaly around 45° N, 150° W (Figure 2a). It should again be noted that this is not simply a linear superposition of the AMV+ and MJO phase 6 responses (since this would, by definition, lead to a response of exactly zero in Figure 4b), but a non-linear modification of the MJO phase 6 response by AMV+. It appears, though, that the altered basic state during AMV+, which itself weakens the Aleutian Low, removes the necessary precondition for the MJO's strengthening of the Aleutian Low after phase 6.

As the Rossby wave initiated by MJO phase 6 continues to propagate eastwards across the extratropics, the NAO tends to shift to its negative phase (Skinner et al., 2022), which the UKESM1 model is able to simulate (cyclonic anomaly around 30° N, 30° W and anticyclonic anomaly around 55° N, 30° W in Figure 4a). During AMV+ this negative NAO response (relative to the basic AMV+ state) is enhanced, though not to the point of being statistically significant, and with a south-west–north-east tilt in its axis (Figure 4b). AMV+ naturally favours a negative NAO, allowing the MJO teleconnection to amplify this response further.

During PDO−, the deepening of the Aleutian Low is completely disrupted (Figures 4e, S1e), with the circulation response to MJO phase 6 not projecting well onto the Aleutian Low. Like the AMV+ case, PDO− generally weakens the climatological low (Figure 2d), giving a less prominent feature onto which the MJO teleconnection can project.

Interestingly, the changes to the MJO teleconnection during PDO+ (Figure 4c) does not mirror the changes seen during PDO−, suggesting a non-linearity in the relationship between the PDO and MJO teleconnections. PDO+ would generally favour a deepened Aleutian Low (Figure 2b; Taguchi et al., 2012). Here, the circulation response to MJO phase 6 does project onto the Aleutian Low, further suggesting that an already deep Aleutian Low is a precondition for the subsequent deepening as a result of MJO phase 6. The change in the circulation response over the Aleutian Low is, however, not significant for PDO+.

PDO+ alters the NAO response to the MJO, though not to a significant extent (Figure 4c). During PDO+, no anticyclonic anomaly is present south-west of Iceland (see negative line contours around 55° N, 30° W in Figure 4c), however there is still a negative NAO-like streamfunction (and hence, by geostrophic balance, pressure) gradient.

AMV− has the smallest impact on the teleconnection in the Aleutian Low region (Figures 4d, S1d). In this case the modification of the response is dominated by the change in Rossby wave source discussed in Section 4.1.1. The resultant wave-like change in the teleconnection results in a strengthening of the negative NAO response. Again, it is worth noting that the impact of AMV− on the teleconnection is not simply the reciprocal of the changes caused by AMV+, providing yet more evidence for the highly non-linear nature of the relationship between MJO teleconnections and low-frequency SST variability.

4.1.3 | Changes in the stratospheric teleconnection pathway

MJO phase 6 would generally lead to a weakened SPV and subsequent negative NAO due to the deepening of the Aleutian Low (Barnes et al., 2019). It would be natural, then, to expect that if this deepening is disrupted, as already discussed for AMV+, this teleconnection would also be disrupted (i.e. the SPV would not be weakened as much by the MJO, and the negative NAO response would be weaker). On the contrary, the SPV weakens slightly more in response to MJO phase 6 during AMV+ (Figure 5), and the negative NAO response is strengthened.

This apparent flipping of the response may be explained by the dependence of the SPV strength on lag. The SPV weakens much earlier than usual (relative to MJO cycle) during AMV+, meaning that it is already in a weakened state

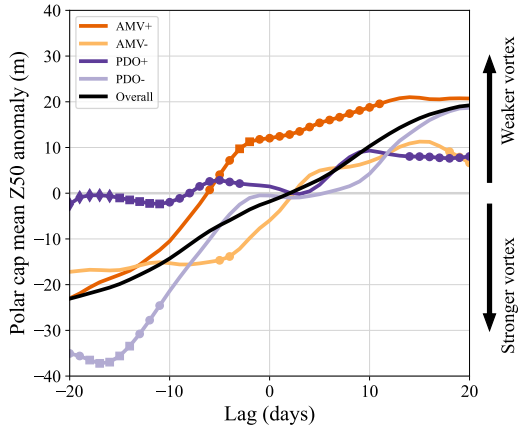

FIGURE 5 Lagged MJO phase 6 composites of polar cap mean (60–90° N) $Z50$ anomalies, for given SST states. Circles, squares, and diamonds indicate that the composite value for a given lag is significantly different from the "Overall" value at the 50%, 80%, and 95% significance level respectively.

when the MJO reaches phase 6. The tropospheric response to MJO phase 4 , which usually features an anticyclonic anomaly across the North Pacific, instead displays a slight deepening of the Aleutian Low at 10-days lag (Figure S1). This shift would not usually occur until MJO phase 6. Taking the gradient of SPV strength between lags 0 and 20 days after MJO phase 6, we see that the weakening actually plateaus, which is more in line with what we would expect. Although we consider MJO phases separately here for the sake of clarity, this result highlights that the response to one MJO phase will itself alter the basic state ahead of subsequent phases.

During PDO+ we observe the opposite effect. Even though the Aleutian Low is deepened, the SPV displays less sensitivity to MJO phase 6. The response to earlier phases also seems to be muted, with the change in SPV strength as a function of lag almost constant. Whilst we do still see a slight weakening of the SPV after MJO phase 6, this is not preceded by additional weakening as we see for other SST states, and so the response is smaller than expected.

A more thorough analysis of the vertical wave activity in the Aleutian low region that facilitates the MJO–SPV teleconnection is required to make further comment on changes to the stratospheric teleconnection pathway. The low statistical significance of the changes in SPV response do, however, highlight that the tropospheric teleconnection pathway is both the dominant pathway, and is more sensitive to decadal scale SST variability.

4.2 | Response to MJO phase 3

MJO phase 3 is designated as enhanced convection in the western Maritime Continent, and suppressed convection in the eastern Maritime Continent (Figure 1c). Following MJO phase 3 we expect a teleconnection pattern resembling a negative PNA (with a weakened Aleutian Low; e.g. Seo and Lee, 2017) and a positive NAO response (e.g. Skinner et al., 2022). The SPV tends to strengthen in the weeks following MJO phase 3, which then favours a positive NAO (Barnes et al., 2019), however this teleconnection pathway is not as strong for phase 3 as it is for phase 6 (Schwartz and Garfinkel, 2017).

4.2.1 | Changes in MJO forcing

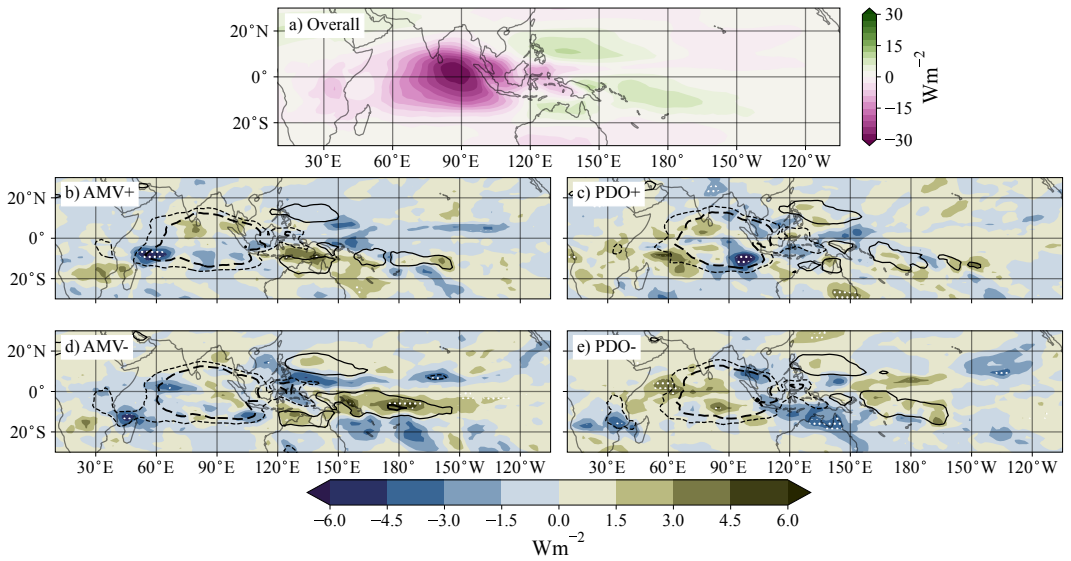

FIGURE 6 Change in OLR anomalies. As in Figure 3, but for MJO phase 3.

During MJO phase 3 the tropical convective anomalies of the MJO itself are not strongly modulated by the SST variability (Figure 6), as we saw for phase 6 in Section 4.1.1. Since SST anomalies are small in the Indian Ocean for all four regimes studied here (Figure 2), it is not surprising that MJO phase 3, in which convection is centred over the eastern Indian Ocean, feels little effect.

4.2.2 | Changes in the extratropics as a result of mean state changes

The UKESM1 piControl simulation captures the expected positive NAO response (anticyclonic anomaly around 40° N, 30° W and cyclonic anomaly around 65° N, 30° W in Figure 7a), though it is slightly weaker than we might expect (Lin et al., 2009). The PNA− response is shifted westward, and whilst a relatively strong anticyclonic anomaly is visible over the Aleutian Islands (50° N, 180° E), consistent with a weakening of the Aleutian Low, the eastern nodes of the PNA quadrupole are clear.

AMV provides little modulation to the extratropical response to MJO phase 3 (Figure 7b and 7d). Though there are small isolated regions in which there is a significant change in the response, this falls within 10% of the spatial domain that we would expect to return a 'false positive' in a significance test at the 90% confidence level. Qualitatively, the teleconnection pattern looks largely similar between Figure 7b and 7d (line contours), and 7a. The only real change of note is an anticyclonic anomaly over western Canada (50° N, 120° W), which appears to form part of a wave-like change in the response as discussed in Section 4.1.1.

The PDO has a greater impact on the response to MJO phase 3 (Figure 7c and 7e). Interestingly, both PDO+ and PDO− appear to compound the weakening of the Aleutian Low (albeit with a slight northward shift in the centre of action during PDO+) that would be expected after MJO phase 3. During PDO− we might expect this type of change, since a weak Aleutian Low is already favoured (Figure 2d). On the other hand, during PDO+ (when we see

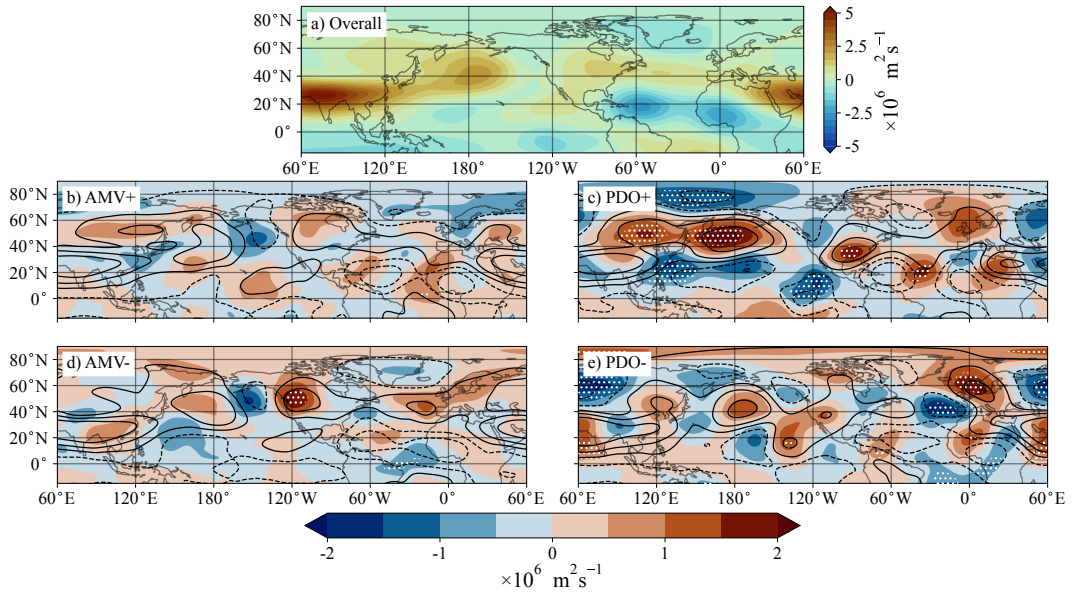

FIGURE 7 Change in lag 10-day ψ250 anomalies. As in Figure 4, but for MJO phase 3.

the larger modification to the response), a stronger Aleutian Low would generally be favoured (Figure 2b). Whilst this seems counter-intuitive initially, a stronger mean Aleutian Low provides a prominent feature onto which the MJO teleconnection can project. This means that a similar relative (to the mean state) weakening of the low will result in a larger absolute change (as we see in Figure 7c).

Whilst PDO+ significantly alters the circulation response to MJO phase 3 over the North Pacific region, it is PDO− that significantly modulates the response over the North Atlantic. We would expect to see a positive NAO response to MJO phase 3, but during PDO− we see a circulation pattern more closely resembling an East Atlantic pattern (Barnston and Livezey, 1987), though it does project slightly onto the negative NAO pattern.

4.2.3 | Changes in the stratospheric teleconnection pathway

The SPV is strengthened slightly after MJO phase 3 (Figure 8), as we would expect (Barnes et al., 2019), however the small gradient of SPV strength as a function of lag (particularly for positive lags), makes determining causality difficult. The signal is also smaller than would be expected from observations, though we would not generally expect this teleconnection to be as robust as the equivalent response to phase 6 (Schwartz and Garfinkel, 2017).

Both AMV states lead to a slightly stronger vortex after MJO phase 3, however in both cases the SPV is already in a strengthened state before MJO phase 3 (see the negative values of polar cap mean $Z50$ anomaly at lag 0). The PDO, however, has little effect on the SPV, with the lag 20 day SPV strength almost identical for PDO± as it is for the overall composite.

In general, MJO phase 3 does not produce a large signal in SPV strength in the UKESM1 model, and this signal is not significantly modulated by the AMV or PDO. Hence it is unlikely that this stratospheric teleconnection pathway contributes much to the modulation of the extratropical tropospheric response to MJO phase 3.

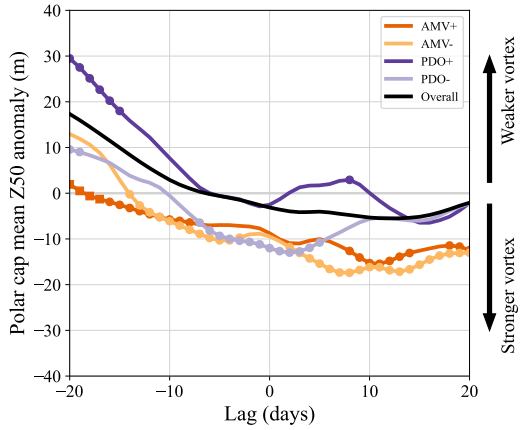

FIGURE 8 Lagged polar cap mean $Z50$ anomalies. As in Figure 5, but for MJO phase 3.

5 | CONCLUSIONS

Both AMV and the PDO cause a statistically significant change in the extratropical response to the MJO in the UKESM1 climate model. By producing lagged MJO composites of upper tropospheric circulation anomaly for each SST state, we show that the response to MJO phases 3 and 6 are modulated by AMV and the PDO, though to varying extents.

AMV alters the extratropical response to MJO phase 6, especially when it is in its positive phase, through changes to the tropospheric Rossby wave pathway, and, to a lesser extent, the stratospheric SPV pathway. The PDO predominantly modulates the MJO phase 6 teleconnection though changes in the Rossby wave response.

Much of the variability observed can be explained though changes in the Aleutian Low's response to the MJO. SST states that favour a deeper Aleutian Low allow the MJO to have a greater impact, whereas SST states that tend to weaken the climatological low in turn inhibit the MJO teleconnection.

The SPV plays a small role in the AMV+ modulation of the MJO phase 6 teleconnection. Whilst the amplified weakening of the SPV during AMV+ is initially unexpected due to the concurrent weakening of the Aleutian Low response, this can be explained by the SPV weakening ahead of MJO phase 6, due to a change in the MJO phase 4 teleconnection. These changes in the SPV response to the MJO, though secondary to the changes tropospheric Rossby wave response, motivate further analysis of the full stratospheric teleconnection pathway, particularly in MJO phases 4–6.

We cannot compare with Skinner et al. (2023) directly, since in their study the AMV and the PDO are acting simultaneously, and the combinations of PDO+/AMV− and PDO−/AMV+ are not prevalent in the UKESM1 model (hence the necessity of restricting the second mode to neutral). There are, however, consistencies which support their hypothesis that decadal modes of SST variability have driven changes in MJO teleconnections over the past 50 years. For example, the shift towards a large anticyclonic anomaly over western North America after MJO phase 6 (around 70° N, 120° W in Figure 3f of Skinner et al. (2023)) is consistent with a shift away from PDO+ (Figure 4), which matches the expected behaviour (Figure S1 of Skinner et al. (2023)). Due to the non-linear nature of the impact of decadal SST variability on MJO teleconnections, there is not a clear shift towards PDO−, though. This highlights the need for further research into the mechanisms behind decadal variability of MJO teleconnections, either through the

use of a wider range of coupled models (e.g. from the CMIP6 project), or through more targeted idealised experiments. Both of these avenues come with limitations due to the persistent under-representation of MJO teleconnections in models (Skinner et al., 2022).

The extratropical response to MJO phase 3 is modulated by the PDO, but not by AMV. Counter-intuitively, both the positive and negative phases of the PDO act to compound the usual weakening of the Aleutian Low after MJO phase 3, however this is due to PDO+ favouring a stronger Aleutian Low, and therefore providing greater scope for this low to weaken as a result of the MJO.

In some of the cases discussed above, a linear superposition of Rossby wave responses seems to occur. That is, the change in the response caused by a different SST state itself resembles a Rossby wave. It is worth reiterating that the differences plotted in panels b–e of Figures 4 and 7 (colour shading) are the modification of the MJO teleconnection by the given SST state, not just a superposition of the responses to the MJO and SST variability. Hence, we hypothesise that this linear Rossby wave-like change in the teleconnections must occur as a result of different Rossby wave modes being excited by the MJO, depending on the SST state. This hypothesis is further supported by the recent work of Dong et al. (2025), who find a shift to a wavenumber-5 Rossby wave response over recent decades.

It is clear that both AMV and the PDO modulate the extratropical response to the MJO on decadal and multi-decadal time scales, and many of the mechanisms behind this modulation have been identified. It must also be noted that biases in the model used will also affect the results obtained. Without longer observational and reanalysis datasets, models remain the most effective way to study variability on decadal time scales. Similar studies with other climate models, or the use of idealised modelling experiments, would help to solidify the robustness of these results.

Since the MJO is used as a source of predictability in the extratropics (e.g. Kent et al., 2022), these results will have impacts on forecasting over the coming decades. As AMV and the PDO modulate the response to the MJO, so the predictability obtained through these responses will also be modified. Similarly, studies of MJO teleconnections in future climates can now use the context provided by these results to more accurately pick apart the changes in the response as a result of internal decadal-scale variability and anthropogenically forced variability.

Acknowledgements

The authors would like to thank Dr Ben Webber and Prof. Tim Woollings for their constructive feedback and discussion during the development of this manuscript. We would also like to thanks Dr. Prince Xavier for providing us with the EOFs from (Wheeler and Hendon, 2004). The research presented in this paper was carried out on the High Performance Computing Cluster supported by the Research and Specialist Computing Support service at the University of East Anglia, and on JASMIN, the UK's collaborative data analysis environment (https://www.jasmin.ac.uk; Lawrence et al., 2013).

Data availability statement

UKESM1 data provided by the CEDA archive (Tang et al., 2019) and accessed through JASMIN (Lawrence et al., 2013). MJO RMM index principal components calculated by Wheeler and Hendon (2004) and provided by Dr Prince Xavier. PDO EOF pattern provided by the NOAA PSL (https://psl.noaa.gov/pdo/).

Author contributions

Daniel Skinner: conceptualization, data curation, formal analysis, investigation, methodology, software, validation, visualisation, writing – original draft, writing – review and editing. **Adrian Matthews:** conceptualization, funding acquisition, investigation, methodology, project administration, resources, software, supervision, validation, writing – review and editing. **David Stevens:** conceptualization, investigation, methodology, project administration, resources, supervision, validation, writing – review and editing.

Supporting information

The following supporting information is available online:

- **Table S1:** The total number of days in which each MJO phase and SST state are active simultaneously.
- **Table S2:** The total number of days in which each MJO phase and SST state are active simultaneously, when the second decadal SST mode is fixed as neutral.
- **Figure S1:** MJO lagged composites of Aleutian Low strength for each MJO phase and SST regime.

references

Ahn, M.-S., Kim, D., Kang, D., Lee, J., Sperber, K. R., Gleckler, P. J., Jiang, X., Ham, Y.-G. and Kim, H. (2020) MJO propagation across the Maritime Continent: Are CMIP6 models better than CMIP5 models? *Geophysical Research Letters*, **47**, e2020GL087250. URL: https://doi.org/10.1029/2020GL087250.

Arcodia, M. and Kirtman, B. (2023) Using simplified linear and nonlinear models to assess ENSO-modulated MJO teleconnections. *Climate Dynamics*, **61**, 5443–5463.

Bao, M. and Hartmann, D. L. (2014) The response to MJO-like forcing in a nonlinear shallow-water model. *Geophysical Research Letters*, **41**, 1322–1328. URL: https://agupubs.onlinelibrary.wiley.com/doi/abs/10.1002/2013GL057683.

Barnes, E. A., Samarasinghe, S. M., Ebert-Uphoff, I. and Furtado, J. C. (2019) Tropospheric and stratospheric causal pathways between the MJO and NAO. *Journal of Geophysical Research: Atmospheres*, **124**, 9356–9371. URL: https://agupubs.onlinelibrary.wiley.com/doi/abs/10.1029/2019JD031024.

Barnston, A. G. and Livezey, R. E. (1987) Classification, seasonality and persistence of low-frequency atmospheric circulation patterns. *Monthly Weather Review*, **115**, 1083–1126. URL: https://journals.ametsoc.org/view/journals/mwre/115/6/1520-0493_1987_115_1083_csapol_2_0_co_2.xml.

Cassou, C. (2008) Intraseasonal interaction between the Madden–Julian Oscillation and the North Atlantic Oscillation. *Nature*, **455**, 523–527. URL: https://doi.org/10.1038/nature07286.

Chen, S., Chen, W., Yu, B., Wu, R., Graf, H.-F. and Chen, L. (2023) Enhanced impact of the Aleutian Low on increasing the Central Pacific ENSO in recent decades. *npj Climate and Atmospheric Science*, **6**, 29. URL: https://doi.org/10.1038/s41612-023-00350-1.

Coburn, J. and Pryor, S. C. (2021) Differential credibility of climate modes in CMIP6. *Journal of Climate*, **34**, 8145–8164. URL: https://journals.ametsoc.org/view/journals/clim/34/20/JCLI-D-21-0359.1.xml.

Deb, P., Matthews, A. J., Joshi, M. M. and Senior, N. (2020) The extratropical linear step response to tropical precipitation anomalies and its use in constraining projected circulation changes under climate warming. *Journal of Climate*, **33**, 7217–7231. URL: https://doi.org/10.1175/JCLI-D-20-0060.1.

Domeisen, D. I. V., Badin, G. and Koszalka, I. M. (2018) How predictable are the Arctic and North Atlantic Oscillations? exploring the variability and predictability of the Northern Hemisphere. *Journal of Climate*, **31**, 997–1014. URL: https://journals.ametsoc.org/view/journals/clim/31/3/jcli-d-17-0226.1.xml.

Dong, C., Peings, Y. and Magnusdottir, G. (2025) Decadal variability of the MJO and implications for southwestern United States wintertime precipitation predictability. *Geophysical Research Letters*, **52**, e2024GL113956. URL: https://agupubs-onlinelibrary-wiley-com.uea.idm.oclc.org/doi/abs/10.1029/2024GL113956.

Esteva-Ingram, T. (2023) *The seasonality of Madden-Julian Oscillation (MJO) Teleconnections*. Masters thesis, University of Oklahoma. URL: https://shareok.org/handle/11244/337928.

Eyring, V., Bony, S., Meehl, G. A., Senior, C. A., Stevens, B., Stouffer, R. J. and Taylor, K. E. (2016) Overview of the Coupled Model Intercomparison Project phase 6 (CMIP6) experimental design and organization. *Geoscientific Model Development*, **9**, 1937–1958. URL: https://doi.org/10.5194/gmd-9-1937-2016.

Feng, P.-N. and Lin, H. (2019) Modulation of the MJO-related teleconnections by the QBO. *Journal of Geophysical Research: Atmospheres*, **124**, 12022–12033. URL: https://agupubs-onlinelibrary-wiley-com.uea.idm.oclc.org/doi/abs/10.1029/2019JD030878.

Franzke, C., Feldstein, S. B. and Lee, S. (2011) Synoptic analysis of the Pacific–North American teleconnection pattern. *Quarterly Journal of the Royal Meteorological Society*, **137**, 329–346. URL: https://rmets.onlinelibrary.wiley.com/doi/abs/10.1002/qj.768.

Fu, Z., Hsu, P.-C. and Liu, F. (2020) Factors regulating the multidecadal changes in MJO amplitude over the twentieth century. *Journal of Climate*, **33**, 9513–9529. URL: https://journals.ametsoc.org/view/journals/clim/33/22/jcliD200111.xml.

Garfinkel, C. I., Benedict, J. J. and Maloney, E. D. (2014) Impact of the MJO on the boreal winter extratropical circulation. *Geophysical Research Letters*, **41**, 6055–6062. URL: https://agupubs.onlinelibrary.wiley.com/doi/abs/10.1002/2014GL061094.

Garfinkel, C. I., Feldstein, S. B., Waugh, D. W., Yoo, C. and Lee, S. (2012) Observed connection between stratospheric sudden warmings and the Madden–Julian Oscillation. *Geophysical Research Letters*, **39**. URL: https://agupubs.onlinelibrary.wiley.com/doi/abs/10.1029/2012GL053144.

Green, M. R. and Furtado, J. C. (2019) Evaluating the joint influence of the Madden–Julian Oscillation and the stratospheric polar vortex on weather patterns in the Northern Hemisphere. *Journal of Geophysical Research: Atmospheres*, **124**, 11693–11709. URL: https://agupubs.onlinelibrary.wiley.com/doi/abs/10.1029/2019JD030771.

Grossmann, I. and Klotzbach, P. J. (2009) A review of North Atlantic modes of natural variability and their driving mechanisms. *Journal of Geophysical Research: Atmospheres*, **114**. URL: https://agupubs.onlinelibrary.wiley.com/doi/abs/10.1029/2009JD012728.

Hall, R. J., Mitchell, D. M., Seviour, W. J. M. and Wright, C. J. (2021) Persistent model biases in the CMIP6 representation of stratospheric polar vortex variability. *Journal of Geophysical Research: Atmospheres*, **126**, e2021JD034759. URL: https://agupubs.onlinelibrary.wiley.com/doi/abs/10.1029/2021JD034759.

Henderson, S. A., Maloney, E. D. and Son, S.-W. (2017) Madden–Julian Oscillation Pacific teleconnections: The impact of the basic state and MJO representation in General Circulation Models. *Journal of Climate*, **30**, 4567–4587. URL: https://doi.org/10.1175/JCLI-D-16-0789.1.

Hurrell, J. W., Kushnir, Y., Ottersen, G. and Visbeck, M. (2003) *The North Atlantic Oscillation: Climatic Significance and Environmental Impact*. Geophysical monograph: 134. American Geophysical Union.

Jenney, A. M., Nardi, K. M., Barnes, E. A. and Randall, D. A. (2019) The seasonality and regionality of MJO impacts on North American temperature. *Geophysical Research Letters*, **46**, 9193–9202. URL: https://agupubs.onlinelibrary.wiley.com/doi/abs/10.1029/2019GL083950.

Jiang, X., Adames, Á. F., Kim, D., Maloney, E. D., Lin, H., Kim, H., Zhang, C., DeMott, C. A. and Klingaman, N. P. (2020) Fifty years of research on the Madden–Julian Oscillation: Recent progress, challenges, and perspectives. *Journal of Geophysical Research: Atmospheres*, **125**. URL: https://doi.org/10.1029/2019JD030911.

Jiang, Z., Feldstein, S. B. and Lee, S. (2017) The relationship between the Madden–Julian Oscillation and the North Atlantic Oscillation. *Quarterly Journal of the Royal Meteorological Society*, **143**, 240–250. URL: https://rmets.onlinelibrary.wiley.com/doi/abs/10.1002/qj.2917.

Kent, C., Scaife, A. A. and Dunstone, N. (2022) What potential for improving sub-seasonal predictions of the winter NAO? *Atmospheric Science Letters*, **n/a**, e1146. URL: https://rmets.onlinelibrary.wiley.com/doi/abs/10.1002/asl.1146.

Kessler, W. S. (2001) EOF representations of the Madden–Julian Oscillation and its connection with ENSO. *Journal of Climate*, **14**, 3055–3061. URL: https://journals.ametsoc.org/view/journals/clim/14/13/1520-0442_2001_014_3055_erotmj_2.0.co_2.xml.

Lawrence, B. N., Bennett, V. L., Churchill, J., Juckes, M., Kershaw, P., Pascoe, S., Pepler, S., Pritchard, M. and Stephens, A. (2013) Storing and manipulating environmental big data with JASMIN. In *IEEE Big Data*.

Le, P. V. V., Guilloteau, C., Mamalakis, A. and Foufoula-Georgiou, E. (2021) Underestimated MJO variability in CMIP6 models. *Geophysical Research Letters*, **48**, e2020GL092244. URL: https://agupubs.onlinelibrary.wiley.com/doi/abs/10.1029/2020GL092244. E2020GL092244 2020GL092244.

Lee, R. W., Woolnough, S. J., Charlton-Perez, A. J. and Vitart, F. (2019) ENSO modulation of MJO teleconnections to the North Atlantic and Europe. *Geophysical Research Letters*, **46**, 13535–13545. URL: https://doi.org/10.1029/2019GL084683.

Li, X., Gerber, E. P., Holland, D. M. and Yoo, C. (2015) A Rossby wave bridge from the tropical Atlantic to west Antarctica. *Journal of Climate*, **28**, 2256–2273. URL: https://journals.ametsoc.org/view/journals/clim/28/6/jcli-d-14-00450.1.xml.

Lin, H., Brunet, G. and Derome, J. (2009) An observed connection between the North Atlantic Oscillation and the Madden–Julian Oscillation. *Journal of Climate*, **22**, 364–380. URL: https://journals.ametsoc.org/view/journals/clim/22/2/2008jcli2515.1.xml.

Lin, J. and Qian, T. (2022) The Atlantic Multi-decadal Oscillation. *Atmosphere-Ocean*, **60**, 307–337. URL: https://doi.org/10.1080/07055900.2022.2086847.

Ling, J., Zhao, Y. and Chen, G. (2019) Barrier effect on MJO propagation by the Maritime Continent in the MJO Task Force/GEWEX Atmospheric System Study models. *Journal of Climate*, **32**, 5529–5547. URL: https://journals.ametsoc.org/view/journals/clim/32/17/jcli-d-18-0870.1.xml.

Madden, R. A. and Julian, P. R. (1971) Detection of a 40–50 day oscillation in the zonal wind in the tropical Pacific. *Journal of Atmospheric Sciences*, **28**, 702–708. URL: https://doi.org/10.1175/1520-0469(1971)028<0702:DOADOI>2.0.CO;2.

— (1972) Description of global-scale circulation cells in the tropics with a 40-50 day period. *Journal of Atmospheric Sciences*, **29**, 1109–1123. URL: https://doi.org/10.1175/1520-0469(1972)029<1109:DOGSCC>2.0.CO;2.

Mantua, N. J. and Hare, S. R. (2002) The Pacific Decadal Oscillation. *Journal of Oceanography*, **58**, 35–44.

Mantua, N. J., Hare, S. R., Zhang, Y., Wallace, J. M. and Francis, R. C. (1997) A Pacific interdecadal climate oscillation with impacts on salmon production. *Bulletin of the American Meteorological Society*, **78**, 1069–1080. URL: https://journals.ametsoc.org/view/journals/bams/78/6/1520-0477_1997_078_1069_apicow_2_0_co_2.xml.

Matthews, A. J., Hoskins, B. J. and Masutani, M. (2004) The global response to tropical heating in the Madden–Julian Oscillation during the northern winter. *Quarterly Journal of the Royal Meteorological Society*, **130**, 1991–2011. URL: https://rmets.onlinelibrary.wiley.com/doi/abs/10.1256/qj.02.123.

Newman, M., Alexander, M. A., Ault, T. R., Cobb, K. M., Deser, C., Lorenzo, E. D., Mantua, N. J., Miller, A. J., Minobe, S., Nakamura, H., Schneider, N., Vimont, D. J., Phillips, A. S., Scott, J. D. and Smith, C. A. (2016) The Pacific Decadal Oscillation, revisited. *Journal of Climate*, **29**, 4399–4427. URL: https://journals.ametsoc.org/view/journals/clim/29/12/jcli-d-15-0508.1.xml.

Pierce, D. W., Barnett, T. P., Schneider, N., Saravanan, R., Dommenget, D. and Latif, M. (2001) The role of ocean dynamics in producing decadal climate variability in the North Pacific. *Climate Dynamics*, **18**, 51–70. URL: https://doi.org/10.1007/s003820100158.

Pohl, B. and Matthews, A. J. (2007) Observed changes in the lifetime and amplitude of the Madden–Julian Oscillation associated with interannual ENSO sea surface temperature anomalies. *Journal of Climate*, **20**, 2659–2674. URL: https://journals.ametsoc.org/view/journals/clim/20/11/jcli4230.1.xml.

Robson, J., Aksenov, Y., Bracegirdle, T. J., Dimdore-Miles, O., Griffiths, P. T., Grosvenor, D. P., Hodson, D. L. R., Keeble, J., MacIntosh, C., Megann, A., Osprey, S., Povey, A. C., Schröder, D., Yang, M., Archibald, A. T., Carslaw, K. S., Gray, L., Jones, C., Kerridge, B., Knappett, D., Kuhlbrodt, T., Russo, M., Sellar, A., Siddans, R., Sinha, B., Sutton, R., Walton, J. and Wilcox, L. J. (2020) The evaluation of the North Atlantic climate system in UKESM1 historical simulations for CMIP6. *Journal of Advances in Modeling Earth Systems*, **12**, e2020MS002126. URL: https://agupubs.onlinelibrary.wiley.com/doi/abs/10.1029/2020MS002126.

Schwartz, C. and Garfinkel, C. I. (2017) Relative roles of the mjo and stratospheric variability in north atlantic and european winter climate. *Journal of Geophysical Research: Atmospheres*, **122**, 4184–4201. URL: https://agupubs.onlinelibrary.wiley.com/doi/abs/10.1002/2016JD025829.

Sellar, A. A., Jones, C. G., Mulcahy, J. P., Tang, Y., Yool, A., Wiltshire, A., O'Connor, F. M., Stringer, M., Hill, R., Palmieri, J., Woodward, S., de Mora, L., Kuhlbrodt, T., Rumbold, S. T., Kelley, D. I., Ellis, R., Johnson, C. E., Walton, J., Abraham, N. L., Andrews, M. B., Andrews, T., Archibald, A. T., Berthou, S., Burke, E., Blockley, E., Carslaw, K., Dalvi, M., Edwards, J., Folberth, G. A., Gedney, N., Griffiths, P. T., Harper, A. B., Hendry, M. A., Hewitt, A. J., Johnson, B., Jones, A., Jones, C. D., Keeble, J., Liddicoat, S., Morgenstern, O., Parker, R. J., Predoi, V., Robertson, E., Siahaan, A., Smith, R. S., Swaminathan, R., Woodhouse, M. T., Zeng, G. and Zerroukat, M. (2019) UKESM1: Description and evaluation of the U.K. Earth System Model. *Journal of Advances in Modeling Earth Systems*, **11**, 4513–4558. URL: https://doi.org/10.1029/2019MS001739.

Seo, K.-H. and Lee, H.-J. (2017) Mechanisms for a PNA-like teleconnection pattern in response to the MJO. *Journal of the Atmospheric Sciences*, **74**, 1767–1781. URL: https://journals.ametsoc.org/view/journals/atsc/74/6/jas-d-16-0343.1.xml.

Seviour, W. J. M., Gray, L. J. and Mitchell, D. M. (2016) Stratospheric polar vortex splits and displacements in the high-top CMIP5 climate models. *Journal of Geophysical Research: Atmospheres*, **121**, 1400–1413. URL: https://agupubs.onlinelibrary.wiley.com/doi/abs/10.1002/2015JD024178.

Skinner, D. T., Matthews, A. J. and Stevens, D. P. (2022) North Atlantic Oscillation response to the Madden–Julian Oscillation in a coupled climate model. *Weather*, **77**, 201–205. URL: https://doi.org/10.1002/wea.4215.

— (2023) Decadal variability of the extratropical response to the Madden–Julian Oscillation. *Geophysical Research Letters*, **50**, e2023GL104576. URL: https://agupubs.onlinelibrary.wiley.com/doi/abs/10.1029/2023GL104576.

Stan, C., Straus, D. M., Frederiksen, J. S., Lin, H., Maloney, E. D. and Schumacher, C. (2017) Review of tropical-extratropical teleconnections on intraseasonal time scales. *Reviews of Geophysics*, **55**, 902–937. URL: https://doi.org/10.1002/2016RG000538.

Taguchi, B., Nakamura, H., Nonaka, M., Komori, N., Kuwano-Yoshida, A., Takaya, K. and Goto, A. (2012) Seasonal evolutions of atmospheric response to decadal SST anomalies in the North Pacific Subarctic Frontal Zone: Observations and a coupled model simulation. *Journal of Climate*, **25**, 111–139. URL: https://journals.ametsoc.org/view/journals/clim/25/1/jcli-d-11-00046.1.xml.

Tang, Y., Rumbold, S., Ellis, R., Kelley, D., Mulcahy, J., Sellar, A., Walton, J. and Jones, C. (2019) MOHC UKESM1.0-LL model output prepared for CMIP6 CMIP piControl. *Earth System Grid Federation*. URL: https://doi.org/10.22033/ESGF/CMIP6.6298. Accessed from the Centre for Environmental Data Analysis (CEDA) archive on 6th October 2021.

Trenberth, K. E. and Shea, D. J. (2006) Atlantic hurricanes and natural variability in 2005. *Geophysical Research Letters*, **33**. URL: https://agupubs.onlinelibrary.wiley.com/doi/abs/10.1029/2006GL026894.

Walters, D., Baran, A. J., Boutle, I., Brooks, M., Earnshaw, P., Edwards, J., Furtado, K., Hill, P., Lock, A., Manners, J., Morcrette, C., Mulcahy, J., Sanchez, C., Smith, C., Stratton, R., Tennant, W., Tomassini, L., Van Weverberg, K., Vosper, S., Willett, M., Browse, J., Bushell, A., Carslaw, K., Dalvi, M., Essery, R., Gedney, N., Hardiman, S., Johnson, B., Johnson, C., Jones, A., Jones, C., Mann, G., Milton, S., Rumbold, H., Sellar, A., Ujiie, M., Whitall, M., Williams, K. and Zerroukat, M. (2019) The Met Office Unified Model Global Atmosphere 7.0/7.1 and JULES Global Land 7.0 configurations. *Geoscientific Model Development*, **12**, 1909–1963. URL: https://gmd.copernicus.org/articles/12/1909/2019/.

Waugh, D. W. and Polvani, L. M. (2010) *The stratosphere: dynamics, transport and chemistry*, vol. 190 of *Geophysical monograph series*, chap. Stratospheric polar vortices, 43–58. American Geophysical Union.

Wheeler, M. C. and Hendon, H. H. (2004) An all-season real-time multivariate MJO index: Development of an index for monitoring and prediction. *Monthly Weather Review*, **132**, 1917–1932. URL: https://doi.org/10.1175/1520-0493(2004)132<1917:AARMMI>2.0.CO;2.

Williams, N. C., Scaife, A. A. and Screen, J. A. (2023) Underpredicted ENSO teleconnections in seasonal forecasts. *Geophysical Research Letters*, **50**, e2022GL101689. URL: https://agupubs.onlinelibrary.wiley.com/doi/abs/10.1029/2022GL101689.

Woollings, T., Charlton-Perez, A., Ineson, S., Marshall, A. G. and Masato, G. (2010) Associations between stratospheric variability and tropospheric blocking. *Journal of Geophysical Research: Atmospheres*, **115**. URL: https://agupubs.onlinelibrary.wiley.com/doi/abs/10.1029/2009JD012742.

Wu, Z. and Reichler, T. (2020) Variations in the frequency of stratospheric sudden warmings in CMIP5 and CMIP6 and possible causes. *Journal of Climate*, **33**, 10305–10320. URL: https://journals.ametsoc.org/view/journals/clim/33/23/jcliD200104.xml.

Yadav, P., Garfinkel, C. I. and Domeisen, D. I. V. (2024) The role of the stratosphere in teleconnections arising from fast and slow MJO episodes. *Geophysical Research Letters*, **51**, e2023GL104826. URL: https://agupubs.onlinelibrary.wiley.com/doi/abs/10.1029/2023GL104826. E2023GL104826 2023GL104826.

Yadav, P. and Straus, D. M. (2017) Circulation response to fast and slow MJO episodes. *Monthly Weather Review*, **145**, 1577–1596. URL: https://doi.org/10.1175/MWR-D-16-0352.1.

Zhang, R. and Delworth, T. L. (2007) Impact of the Atlantic Multidecadal Oscillation on North Pacific climate variability. *Geophysical Research Letters*, **34**. URL: https://agupubs.onlinelibrary.wiley.com/doi/abs/10.1029/2007GL031601.

Zhou, W. and Xie, S.-P. (2017) Intermodel spread around the Kuroshio–Oyashio Extension region in coupled GCMs caused by meridional variation of the westerly jet from atmospheric GCMs. *Journal of Climate*, **30**, 4589–4599. URL: https://journals.ametsoc.org/view/journals/clim/30/12/jcli-d-16-0831.1.xml.

Zhou, Y., Wang, S., Fang, J. and Yang, D. (2023) The Maritime Continent barrier effect on the MJO teleconnections during the boreal winter seasons in the northern hemisphere. *Journal of Climate*, **36**, 171–192. URL: https://journals.ametsoc.org/view/journals/clim/36/1/JCLI-D-21-0492.1.xml.

GRAPHICAL ABSTRACT

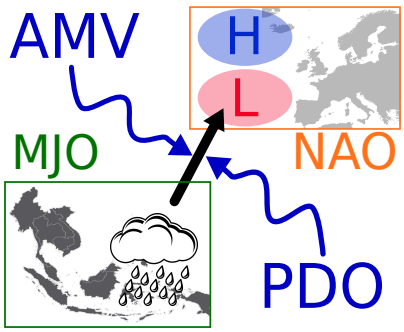

The Madden–Julian Oscillation (MJO) is a key predictor of extratropical weather, such as the North Atlantic Oscillation (NAO), through its teleconnection patterns. These teleconnection patterns are known to vary over a range of timescales, but the way in which they vary on decadal time scales is not well understood. Here we show, using the UKESM1 coupled climate model, that both Atlantic Multi-decadal Variability (AMV) and the Pacific Decadal Oscillation (PDO) can modulate MJO teleconnections.